JBC Papers in Press. Published on July 10, 2019 as Manuscript RA119.009531
The latest version is at http://www.jbc.org/cgi/doi/10.1074/jbc.RA119.009531

Recombinant mussel protein Pvfp-5β: a potential tissue bioadhesive

Radha Santonocito[1#], Francesca Venturella[2,4#], Fabrizio Dal Piaz[3], Maria Agnese Morando[4], Alessia Provenzano[1], Estella Rao[1], Maria Assunta Costa[1], Donatella Bulone[1], Pier Luigi San Biagio[1], Daniela Giacomazza[1], Alessandro Sicorello[5], Caterina Alfano[4*], Rosa Passantino[1*], Annalisa Pastore[5]

[1]Istituto di Biofisica- Consiglio Nazionale delle Ricerche, Palermo, Italy
[2]University of Palermo, Palermo, Italy
[3]University of Salerno, Italy
[4]Fondazione Ri.MED, Palermo, Italy
[5]King's College London, London, UK5

*Co-corresponding authors
calfano@fondazionerimed.com
rosa.passantino@cnr.it

#The two authors have contributed equally

Keywords: adhesion proteins, biomaterials, marine proteins, recombinant proteins, structure
Running title: Characterization of the recombinant mussel protein Pvfp-5

Abstract

During their lifecycle, many marine organisms rely on natural adhesives to attach to wet surfaces for movement and self-defence in aqueous tidal environments. Adhesive proteins from mussels are biocompatible and elicit only minimal immune responses in humans. Therefore these proteins have received increased attention for their potential applications in medicine, biomaterials and biotechnology. The Asian green mussel *Perna viridis* secretes several byssal plaque proteins, molecules that help anchor the mussel to surfaces. Among these proteins, protein-5β (Pvfp-5β) initiates interactions with the substrate, displacing interfacial water molecules before binding to the surface. Here, we established the first recombinant expression in *Escherichia coli* of Pvfp-5β. We characterized recombinant Pvfp-5β, finding that despite displaying a CD spectrum consistent with features of a random coil, the protein is correctly folded as indicated by MS and NMR analyses. Pvfp-5β folds as a β-sheet–rich protein as expected for an epidermal growth factor (EGF)-like module. We examined the effects of Pvfp-5β on cell viability and adhesion capacity in NIH-3T3 and HeLa cell lines, revealing that Pvfp-5β has no cytotoxic effects at the protein concentrations used and provides good cell-adhesion strength on both glass and plastic plates. Our findings suggest that the adhesive properties of recombinant Pvfp-5β make it an efficient surface coating material, potentially suitable for biomedical applications including regeneration of damaged tissues.

Introduction

It was proposed in the '90ies that animals such as mussels, sandcastle worms and geckos, are great potential sources of nontoxic adhesive biomaterials which have the additional advantage to be suited for wet environments (1, 2). These strong and water-insoluble adhesion properties have attracted increasing interest for potential applications in regenerative medicine, biotechnology and material science (3-6). In particular, mussels have received significant attention especially because of their ability to adhere so tightly to their

substrates to resist also turbulent tidal condition (7-9). Mussel adhesion is possible through the secretion of a protein-based holdfast (byssus) which has evolved to anchor the mussel shell to underwater rocks and other substrates (10-12). The byssus consists of a bundle of threads intertwined together and forming a filament (13, 14). The end of each thread forms an adhesive plaque that contains a water-resistant glue and allows anchoring to entirely different substrates including glass, Teflon, metal, and plastic (15, 16). Chemically, the byssus is composed of mussel adhesion proteins which are synthesised in the mussel foot. Six mussel foot proteins (mfps) have been identified in the Mytilus genus (mfp-2, -3S, -3F, -4, -5 and -6) (17). A particularly attractive property of these proteins is their inherent biodegradable nature which makes them environmentally friendly (18). They are also good candidates as medical adhesives since are usually nontoxic to the human body and do not easily elicit strong immune response (19-22). Mfps are thought to acquire their adhesive properties through a post-translational modification that consists in the enzymatic hydroxylation of tyrosine to 3,4-dihydroxyphenyl-L-alanine (DOPA) (23). In a recent study the abundance and proximity of catecholic DOPA and lysine residues suggest a synergistic interplay in adhesion (24). DOPA residues enable cross-linking of the proteins by oxidative conversion to *o*-quinone resulting in the filamentous byssus (25-27). Although preliminary studies have suggested that mussel adhesion protein analogues without DOPA have reduced ability for adhesion, firm confirmation of these result is still lacking because of the insufficient characterization of the proteins, especially in their non-DOPA bound form because of difficulties in producing the proteins in their recombinant form.

Three mfps were recently identified in the Asian green mussel *Perna viridis* (28-30) foot by RNA-sequencing integrated with proteomic analysis (31): Pvfp-3, Pvfp-5β and Pvfp-6. They have molecular weights ranging between 5.3-11.2 kDa. Saline-induced adhesive secretions from mussel foot of *P. viridis* showed that, among them, Pvfp-5β variant in the 8-10 kDa range is secreted first, typically within 10 s after saline injection. It was hypothesized that this protein is also the first protein to initiate interaction with the substrate making it a system of particular interest (32). Sequence analysis identified two tandem EGF motifs along the Pvfp-5β amino acid sequence which shares 47-50% identity with the EGF repeats of the Notch ligand delta-like 1 protein (33). Such elevated identity makes it convincing to expect a tight similarity of the fold. EGF motifs are all- β proteins that are characterized by three conserved disulphide bridges. The presence of EGF-like modules in mfps is not unique of Pvfp-5β since other mussel adhesive proteins of various species, such as Mgfp-2 of *Miytilus galloprovincialis,* have several copies of EGF-like motifs (34, 35).

In this study, we describe the first implementation of the successful production of recombinant Pvfp-5β and its characterization by Circular Dichroism (CD), Nuclear Magnetic Resonance (NMR), and Dynamic Light Scattering (DLS). We show that the protein, which was produced as inclusion bodies, can be refolded in a species with the disulfide bridges expected on the basis of sequence homology correctly formed. We also prove for the first time that, despite having features which are not typical of an all-β protein, Pvfp-5β folds as a β-rich protein as expected for an EGF-like module. We analysed in detail the aggregation and adhesion properties of Pvfp-5β as part of a longer-term involvement aiming at the characterization of mfp-based biomaterial. Our results show that Pvfp-5β has intrinsic adhesive properties also in the absence of DOPA attachment. These properties make the protein an excellent and efficient surface coating material which could be used for biomedical applications including the regeneration of damaged tissues.

Results

Finding the conditions for reproducible production of recombinant HT-Pvfp-5β

Several attempts were done to optimize the production of recombinant Pvfp-5β as this is the prerequisite of any future study on this protein. Recombinant Pvfp-5β was first expressed as a thioredoxin fusion protein with a TEV cleavable site just before the Pvfp-5β (phTt-Pvfp-5β). The protein expressed in inclusion bodies from which it was solubilised under denaturing and reducing conditions in 8 M urea and refolded by slowly removing the denaturing agent dialysing in phosphate buffer at pH 7.4. This did not result in a correctly folded sample as judged by mass spectrometry analysis (data not shown). The construct was then modified and subcloned as a TEV protease cleavable N-terminal His-tag protein (HT-Pvfp-5β) which, although still resulting in inclusion bodies, would allow us to exclude unwanted tags. After solubilising the inclusions bodies, purification was carried out under denaturing conditions with a single step affinity purification by immobilized-metal affinity chromatography (IMAC) since HT-Pvfp-5β was already relatively pure in the washed inclusion bodies (**Figure S1A,B**). To allow correct refolding of the protein, urea was gradually removed by sequential dialysis in the presence of both reduced and oxidized glutathione. A final dialysis was performed in 5% acetic acid. An acidic pH mimics the conditions observed in the distal depression cavitation during mussel adhesion (17). His-tag removal by TEV protease digestion was achieved in phosphate buffer at pH 7.4 or sodium acetate buffer at pH 5.6 (**Figure S1C, lanes 2 and 3**). All the experiments described hereafter were repeated with and without the tag. We did not observe noticeable differences (data not shown). We decided to show the data obtained with the tagged protein for consistency and historical reasons. The apparent molecular weight of HT-Pvfp-5β on SDS-PAGE was 13 kDa versus the predicted molecular mass of 9.4 kDa. The difference is likely the consequence of the basic pI value (9.2) and a possible non globular shape of the protein.

Identification of the disulfide patterns by mass spectrometry

A mass spectrometry-based approach on the final product was used to characterize the disulphide bond pattern of the protein. ESI-MS analysis of carboxy-amidomethylated HT-Pvfp-5β indicated that only two of the twelve cysteines were not involved in disulphide bridges (measured molecular weight 12021.1, theoretical molecular weight of tetra-carboxyamidomethylated HT-Pvfp-5β carrying 5 disulphide bridges 12020.6). Enzymatic digestion of the modified protein and the subsequent LC-MS/MS analysis of the resulting peptides allowed description of the coupling of the other ten cysteines (**Table 1 and Figure 1A**): identification of the disulfide-bridged peptides (32-34)-(49-50) indicated of the presence of a covalent bond involving Cys33 and Cys49. Similarly, the peptides (51-52)-(59-62), (63-66)-(72-78), (67-71)-(87-88) and (89-91)-(97-100) were detected, demonstrating the presence of the disulfide bridges Cys51-Cys60, Cys65-Cys76, Cys70-Cys87 and Cys89-Cys98, respectively. Cys28 and Cys39 were not involved in a disulfide bridge and were found as carboxyamidomethylated peptides 24-31 and 35-40, respectively.

These results are fully consistent with what is expected for a protein that has a high homology with two tandem EGF-like motifs (**Figure 1A**). According to a Blast search in PDB, the sequence with higher degree of sequence identify (47%) is that of the Notch ligand delta-like 1 protein (4xbm) (38) (residues 288-368). In the two tandem EGF domains of 4xbm are observed only five disulphide bridges of the six expected for these motifs (**Figure 1B**). The sixth bridge between Cys332 and Cys343 is not formed since the two cysteines are slightly too far (4.5 Å apart S-S distance) but still relatively close. The results from

spectrometry mapped onto a model built using 4xbm as a template indicated that most the disulphide bridges of HT-Pvfp-5β match those observed in 4xbm. However, the N-terminal one is not formed possibly because too close to the fraying edge of the domain (**Figure 1C**). Interestingly, the conformation of the linker between the two EGF motifs which contains Cys65 does not allow formation in the model of the sulfur bridge Cys65-Cys76 as the consequence of a two residue deletion. Since we observe it experimentally, we must deduce that the accuracy of the homology modelling in this region is low. A more realistic model might be obtained by imposing in the modelling the sulfur bridge as a restraint.

Probing the fold of recombinant HT-Pvfp-5β

We then investigated the secondary and tertiary structure of HT-Pvfp-5β. Far-UV CD spectra of the protein dissolved in 5% acetic acid (pH 2.0) exhibited a negative peak at 200 nm and a weak positive maximum at 230 nm, the latter probably caused by the high content of tyrosines (17.5%) **(Figure 2A).** Spectral deconvolution gave predominant content of β-sheet and random coil conformations **(Table S1**). The effect of pH on the CD spectrum of HT-Pvfp-5β was investigated in the range 2.0-5.6. The spectra did not change except for a minor increase of the maximum at 230 nm and a small deepening of the minimum at 200 nm at less acidic pH. The spectrum is very similar to that published for HT-Pvfp-5β directly purified from mussels (32), confirming that the recombinant protein has properties similar to those observed for the protein from natural sources. Since however the CD spectra are far from what is expected for a predominanly β-sheet protein (39), we considered these results inconclusive for deciding whether the protein has the EGF-like fold expected. We resorted instead to NMR spectroscopy. We recorded a ^{1}H two-dimensional NOESY spectrum of HT-Pvfp-5β which showed an excellent distribution of resonances with amide protons resonating up to 9.6 ppm and ring current shift effects that are typical of a well folded protein with a defined hydrophobic core **(Figure 2B)**. The spectrum also revealed several clearly defined connectivities directly left to the water signal (5-6 ppm) as expected for a β-rich protein such as EGF-like domains (40). The general appearance of the spectrum is that expected for a non-aggregated protein. Similar conclusions were supported by HSQC spectrum (**Figure 2C)** where it is possible to count 90 peaks out of the 95 expected. Apart from some expected changes in the chemical shifts, no other drastic changes in the general dispersion and linewidths were observed in the range of pH 2.0-7.4 that could indicate aggregation (data not shown). Thus, our data directly support for the first time the prediction so far solely based on sequence similarity that the Pvfp-5β protein is able to fold as a stable EGF-like domain.

Surface coating using HT-Pvfp-5β

We then investigated the surface coating ability of purified HT-Pvfp-5β. The method is based on the observation that mfps come out of solution as pH is raised and spontaneously adsorb and coat to the first surface they contact. Three surfaces normally used in cell culture were tested: a hydrophilic surface (tissue culture treated polystyrene (or TCT-PS) 96-well plate), a hydrophobic surface (untreated polystyrene (or TCUT-PS) 96-well plate) and a tissue culture treated glass 96-well plate (TCT-G). Cell-Tak, a natural extract of *M. edulis* adhesive-protein mixture of mfp-1 and -2, and uncoated wells were used as positive and negative controls respectively. Adsorption and coating of HT-Pvfp-5β and Cell-Tak in 5% acetic acid were performed based on the Cell-Tak manufacturer's instruction (adsorption method) adding sodium bicarbonate at pH 8.3. HT-Pvfp-5β showed remarkable coating ability for all surfaces (**Figure 3**). A staining more pronounced than with Cell-Tak was observed on both polystirene surfaces.

pH-induced self-assembly of HT-Pvfp-5β

We reasoned that, given the observed coating properties, it would be reasonable to assume that Pvfp-5β has a tendency to self-assemble. On the other hand, the protein is clearly stable in a wide range of concentrations as judged both by CD and NMR. We tried to identify the conditions that could promote aggregation in the coating assay using DLS and followed the behaviour of the protein in aqueous solution at each step of the surface coating protocol. HT-Pvfp-5β (125 µM) proved to be fully soluble in a 5% acetic acid aqueous solution at pH 2. No signal of the autocorrelation function was detectable by DLS measurements as expected for a well dispersed solution of a protein with a hydrodynamic radius of only a few Å. No signal was detected after dilution, up to 19 µM. Upon addition of an appropriate amount of 0.1 M sodium bicarbonate at pH 8.3, the pH suddenly changed to 6.8 due to generation of CO_2. Under these conditions of pH shock, small objects of about 10 nm were observed after a few minutes. They remained stable until approximately 400 minutes. After that, a sudden increase of intensity and size was simultaneously observed. The curve profile was typical of a phase transition triggered by a sufficient concentration of critical nuclei formed during the lag phase (supersaturation) (**Figure 4**). At the end of the aggregation kinetics, the sample showed a heterogeneous population of low and high molecular weight objects as confirmed by SEM imaging (data not shown). These results suggest a propensity of the protein to aggregate under conditions of pH shock.

Cell proliferation on different HT-Pvfp-5β coated surface

The surface coating ability of HT-Pvfp-5β led us to investigate the effect of HT-Pvfp-5β coating on cell proliferation and viability. To assess this, we performed the MTS assay, a colorimetric method for sensitive quantification of viable cells in proliferation and cytotoxicity. The method is based on the reduction of the MTS tetrazolium compound by viable cells (41). This reaction generates formation of a colored formazan product in cell culture media that is induced by NAD(P)H-dependent dehydrogenase enzymes. The assay was performed throughout 72 h of cell growth. Absorbance of the formazan dye produced in the cell culture plates was evaluated in triplicates in a micro plate reader at 490-nm wavelengths. The obtained absorbance values were directly proportional to the number of viable cells in the culture. Cells were seeded into uncoated or HT-Pvfp-5β coated wells of TCT-PS 96-well plates. Both NIH-3T3 and HeLa cells remained viable for 72 h after being into contact with HT-Pvfp-5β. No statistically significant differences were observed between uncoated or coated with HT-Pvfp-5β wells, indicating no cytotoxic effects of HT-Pvfp-5β coating (**Figure 5**).

Cell adhesion and spreading of HT-Pvfp-5β

Finally, we investigated whether the protein promotes cell-adhesion or has spreading abilities. A cell adhesion assay was performed on different surfaces (glass and polystyrene) with HT-Pvfp-5β coating, Cell-Tak coating, PLL coating (positive control) and non-coating (negative control). HeLa and NIH-3T3 cells were diluted in serum-free medium to eliminate exogenous cell attachment and spreading factors, and seeded into uncoated and coated wells of TCT-PS, TCUT-PS and TCT-G 96-well plates. After 2 h of cell-adhesion, the unattached cells were aspirated gently and rinsed with PBS. The MTS assay was performed to measure the living-cell adhesion quantitatively. HT-Pvfp-5β exhibited better cell-adhesion ability than PLL and Cell-Tak on glass and polystyrene plate with both cell lines. The number of adherent NIH-3T3 cells increased by about 4.2-6 folds on HT-Pvfp-5β coated glass surface compared to the uncoated glass

(**Figure 6A**) and by 1.5-2.3 folds on HT-Pvfp-5β coated polystyrene surfaces (**Figure 6B and C**). Although HeLa cells appeared more spread on all surfaces coated with HT-Pvfp-5β the number of adherent cells was higher only on HT-Pvfp-5β coated tissue-culture untreated polystyrene surfaces (1.8-1.9 folds) (**Figure 6A, B and C**).

After cell-attachment on surface, cells underwent morphologic changes and spreading with an active reorganization of the cytoskeleton. This is due to actin polymerization from a monomeric G-actin form to the filamentous polymeric F-actin form which causes rearrangements characterized by formation of protrusion including filopodia and lamellipodia. To study whether the adhesive substrate HT-Pvfp-5β was capable of supporting spreading, F-actin was stained to observe the cytoskeleton. HeLa and NIH-3T3 cells were seeded in serum-free medium, into uncoated, PLL or HT-Pvfp-5β coated glass wells of an 8-well Nunc Lab-Tek II chamber slide. Unattached cells were aspirated and the adhesion state and spreading of attached cells were analyzed by actin staining by the green-fluorescent Alexa Fluor™ 488 Phalloidin and fluorescence microscopy. A higher quantity of adherent cells with a more organized cytoskeleton were observed on HT-Pvfp-5β coating in both HeLa and NIH-3T3 cells if compared to the poorly spread cells on PLL coated wells (**Figure 7 and Table S2**). In contrast, on uncoated surface cells were not spread and F-actin was concentrated along the plasma membrane. These results show that coating of HT-Pvfp-5β is biocompatible and significantly affects cell attachment and spreading.

Discussion

The development of new biomaterials has a prominent role which has lately attracted increasing interest for applications in regenerative medicine, biomaterials and biotechnology. It is not an easy task since, ideally, a polymeric scaffold in biomaterial engineering should have several important features which do not admit a compromise: they should i) hold appropriate surface properties promoting cell adhesion, proliferation and differentiation, ii) be biocompatible and biodegradable, iii) have high porosity and a high surface-area to volume ratio, with an interconnected pore network for cell growth and flow transport of nutrients and metabolic waste, and iv) have specific mechanical properties.

Here, we presented a study in which we have characterised Pvfp-5β, one of the main components of the byssus of *Perna viridis*. We first set up a scheme for the production of the recombinant protein since this possibility is the prerequisite to produce in the future suitable quantities of the protein without the ordeal of having to purify it directly from mussels. Recombinant production also provides higher flexibility to obtain the protein with and without post-translational modifications and thus the possibility to distinguish the intrinsic properties of the protein from those of the post-translational modifications. The endeavour was not straightforward since Pvfp-5β contains 12 cysteines, which constitutes as much as the 15% of its composition. Despite the considerable advancements in the production of cysteine-rich proteins, the task remains challenging. After trying different constructs and optimising the conditions, we found that a suitable strategy is the expression of the protein in inclusion bodies and its refolding in the presence of glutathione.

This meant that we could, for the first time, characterise the protein in its non-DOPA bound form. We found that refolded HT-Pvfp-5β is able to adopt a native conformation with correct pairing of the sulfur bridges according to an EGF-like module as supported by mass spectrometry and NMR studies. This evidence is new because, while our spectrum is in perfect agreement with that of Pvfp-5β directly purified from mussels(32), previous studies were based only on CD data which, for a protein with an EGF fold, are inconclusive:

as observed in model compounds, a CD spectrum with a minimum around 195 nm and a small positive band around 215 nm is the hallmark of a random coil conformation(39). This should be compared with the CD spectrum of a β-protein which should have a minimum around 215 nm. However, it is well known that in some small well folded all β-sheet proteins such as EGF- and SH3-like domains(42), the CD spectrum is something intermediate between that of a random coil and a β-sheet conformation. This peculiarity is probably the consequence of the combination of internal dynamics, the presence of π-π stacking interactions between aromatics(39) and other similar factors. This is precisely the spectrum we observed for HT-Pvfp-5β.

To prove a β-rich fold, we resorted instead to NMR. The NMR spectrum of HT-Pvfp-5β has all the features of a folded protein, eliminating any doubt that refolding could have been unsuccessful. The homo-nuclear 2D NOESY spectrum also supports the presence of a significant β-sheet content as expected for an EGF-like fold. We are thus confident that the recombinant protein can be used for further studies as a much more ductile substitute of the protein from natural sources.

We characterized the protein for its adhesion and cytotoxicity. Interestingly, we could show that HT-Pvfp-5β retains considerable adhesion properties also in the absence of DOPA. This suggests that these properties are an inherent feature of this mfp rather than solely depending on the presence of DOPA. We also demonstrated that the protein has no tendency to aggregate at acidic conditions whereas it can readily self-assemble under specific stress conditions. This behaviour is generally observed in mfps because of their high levels of aromatic and basic amino acids (43) and is probably a key element to determine the adhesion properties of Pvfp-5β. Finally, we demonstrated that recombinant Pvfp-5β is non-toxic as requested for a biomaterial. Taken together, our study proposes Pvfp-5β as a potential source of biomaterial. Future studies, already on-going in our laboratory, will clarify the biodegradability and the mechanical properties of Pvfp-5β and undertake a detailed comparison of the properties of the native and the post-translationally modified protein.

Experimental Procedures

Expression and purification of recombinant protein HT- Pvfp-5β

Cloning was achieved as detailed in Suppl. Materials. *E. coli* BL21-Gold(DE3) cells (Agilent Technologies) were grown in Luria-Bertani (LB) medium with 50 μg ml^{-1} ampicillin (Sigma-Aldrich) and transformed with the vector expressing the recombinant Pvfp-5β as a TEV (Tobacco Etch Virus) protease cleavable N-terminal His-tag protein (HT-Pvfp-5β). When OD_{600} of the culture reached 0.6-0.8, expression was induced by 1 mM isopropyl-b-D-thiogalactopyranoside (IPTG) for 3 h at 37°C and 250 rpm. The harvested cell pellet was washed twice with 100 mM Tris-HCl, 10 mM EDTA, 5 mM $CaCl_2$ (pH 7.4) and then with 20 mM sodium phosphate buffer at pH 7.4. The cell pellet was resuspended in pre-chilled lysis buffer (20 mM sodium phosphate buffer at pH 7.4, 500 mM NaCl, 2 mM DTT, $MgCl_2$ 5 mM, cOmplete EDTA free protease inhibitor-Roche mixture, 10 μg/ml DNase and 0.5 mg/ml lysozyme). The cells were disrupted on ice by ultrasonic homogenizers (Bandelin HD 2070), and incubated 30 min at 4°C. The inclusion bodies containing expressed recombinant HT-Pvfp-5β were washed twice in lysis buffer with 1% Triton X-100, followed by one wash in the same buffer. The washed inclusion bodies were solubilized for 2 h at room temperature then overnight at 4°C in 8 M urea, 1 M NaCl, 2 mM DTT, 20 mM sodium phosphate buffer at pH 7.4. The supernatant was collected after centrifugation at 20,000 g, 4 °C for 30 min, filtered using 0.45 μm filter (Sartorius Stedim Biotech) and loaded onto a 5 ml

HisTrap FF crude column prepacked with Ni-Sepharose (GE Healthcare Life Sciences) equilibrated in the same buffer of the protein sample. The His-tagged protein was eluted under denaturing and reducing conditions with a linear gradient from 0 to 500 mM of imidazole in 10 CV at room temperature. Refolding of the eluted protein was then performed by sequential extensive dialysis at 4°C, firstly in 20 mM sodium phosphate at pH 7.4, 2 M urea, 250 mM NaCl, 2 mM reduced gluthatione (GSH) and 0.5 mM oxidised gluthatione (GSSG), then in the same buffer with no urea. Refolded HT-Pvfp-5β was lastly dialyzed in 5% acetic acid and lyophilized. Protein purity was verified by 14% (w/v) SDS-PAGE and Coomassie brilliant blue staining and resulted > 90%. Protein concentration was assessed by spectrophotometric determination at 280 nm (extinction coefficient [ε] = 27570). The final yield was about 4.3 mg of protein per each gram of cell pellet for the unlabeled protein and about 1.6 mg of protein per each gram of cell pellet for the 15N-labeled protein.

Disulphide bridge characterization

The disulphide bridges of refolded HT-Pvfp-5β were identified by the combined use of proteolytic digestion and mass spectrometry. The freeze-dried protein (10 nmol) was dissolved in 0.1 mM HCl (pH 4), diluted in 100 mM ammonium bicarbonate (final pH 7.5) and incubated with a 100-fold molar excess of iodoacetamide for 30 min in the dark to achieve covalent modification of the cysteine residues not involved in disulphide bonds. The reaction was stopped by removing the unreacted iodoacetamide by SPE cartridge (Chromabond HRX-Macherey-Nagel). An aliquot (0.5 nmol) of the modified HT-Pvfp-5β underwent LC-MS analysis on a Q-TOF premier instrument coupled with an Alliance 695 HPLC pump (Waters) to determinate the number of modified cysteines and verify the homogeneity of the reacted protein. The protein was loaded on an Aeris C4 (150x 2.1 mm) column (Phenomenex) and eluted performing a gradient from 20% to 80% of acetonitrile over 5 minutes. Mass spectra were acquired in positive ion mode over the 1500–3000 m/z range. The modified protein was then lyophilised, dissolved in 100 mM ammonium bicarbonate (pH 7.5) and incubated with proteomic-grade trypsin (enzyme:protein ratio 1:50 w/w) at 37 °C. After 6 h of reaction, chymotrypsin (enzyme:protein ratio 1:100 w/w) was added to the mixture and the digestion proceeded for further 2 h and stopped by lowering the pH to 2 with 1 M HCl. Resulting fragments were analysed by the LC-MS system. Peptide separation was achieved with a Aeris C18 (150x 2.1 mm) column (Phenomenex) and a gradient from 5% to 65% of acetonitrile over 30 min. Mass spectra were in positive ion mode over the 500–2000 m/z range; most abundant species underwent MS/MS analyses. Mass and MS/MS spectra were analysed by the Masslynx software (Waters). The analysis was repeated on ten independently produced samples to test reproducibility.

Structural characterization

CD studies were carried out with a J-815 (Jasco, Tokyo, Japan) spectropolarimeter using a quartz cell with 0.1 mm path length. Spectra were recorded at 20 °C with a scan rate of 100 nm/min overaged over five times. The final concentration of the tested protein was 34 μM. All spectra were corrected by subtracting the spectra of the solvent.

NMR spectra were recorded at 25°C on a Bruker AVANCE III TM HD operating at 600 MHz ^{1}H frequency. A NOESY spectrum was recorded on 250 μM sample in H_2O/D_2O at pH 2.4 using a mixing time of 150 ms. HSQC spectra measurements were carried out using a ^{15}N uniformly labeled protein at a concentration of 250 μM and different pH values (from 2.4 to 7.4). The spectra were processed using the NMRPipe program (36).

DLS measurements were performed using a Brookhaven Instrument BI200-SM goniometer with temperature controlled by a thermostatic recirculating bath. The light scattered intensity and time autocorrelation function (TCF) were measured at 90° scattering angle by a Brookhaven BI-9000 correlator and a 50 mW He-Ne laser tuned at $\lambda = 632.8$ nm. The correlator operated in the multi-τ mode and the experimental duration was set to >2000 counts on the last channel of the correlation function. Data were fit by the cumulant method(37) to derive a z-averaged translational diffusion coefficient, which was converted to an average apparent hydrodynamic radius of an equivalent sphere, R_h, through the stoke-Einstein relationship $D_z = kT/6\pi\eta R_h$ (where k is the Boltzmann's constant, T the absolute temperature, η the viscosity, and D_z the translational diffusion coefficient). Before DLS measurements, all solutions were filtered through 0.2 µm cellulose acetate (Millipore) syringe filters to remove high molecular species. CD, DLS and NMR measurements were recorded on independent protein preparations to compare the homogeneity of the samples and confirm reproducibility.

Surface coating

Tissue culture treated (hydrophilic surface) (Corning) and untreated (hydrophobic surface) (Greiner Bio-One International) polystyrene 96-well plates (TCT-PS and TCUT-PS respectively), and tissue culture treated SensoPlate Plus glass bottom 96-well plates (TCT-G) (Greiner Bio-One International), were coated with HT- Pvfp-5β or Cell-Tak (BD Bioscience), a natural extract of mfps. The amounts of coating material used was 7 µg/cm^2 of well area. Cell-Tak and uncoated wells were used as positive and negative controls respectively. Coating with HT-Pvfp-5β and Cell-Tak were performed based on the Cell-Tak manufacturer's instruction (adsorption method). The appropriate amount of Cell-Tak or HT- Pvfp-5β dissolved in 5% acetic acid was diluted with Milli-Q water up to 19 µM, 10 µl were placed into each well, and mixed with three-fold volumes of neutral buffer solution (0.1 M sodium bicarbonate, pH 8.3). After incubation at room temperature for 10-16 h, the solution was aspirated. Wells were washed thoroughly with sterile Milli-Q water for 1 h. The coating of attached proteins was visualized by Coomassie-blue staining. Five independent experiments were performed with two replicates per each sample.

Mammalian cell culture

Human HeLa (ACC-673–DSMZ) and murine NIH 3T3 (SIGMA-ALDRICH) cell lines were cultured in Dulbecco's Modified Eagle Medium (DMEM)-high glucose supplemented with 10% fetal bovine serum (FBS) and 10% bovine calf serum (BCS), respectively, 1% penicillin and streptomycin (10,000 U/mL and 10,000 µg/mL, respectively) at 37°C and 5% CO_2 humidified air. Cells were treated with trypsine (SIGMA-ALDRICH) at 80% confluency using the standard protocol, and resuspended into new culture flasks. Cells were passaged every third day.

Cell proliferation, adhesion and spreading on HT-Pvfp-5β coated surface

Cell viability and proliferation were examined by CellTiter 96® AQueous One Solution Cell Proliferation Assay-(MTS) (PROMEGA). NIH-3T3 and HeLa cells were diluted in serum-containing medium, and seeded into uncoated or HT- Pvfp-5β coated wells of TCT-PS 96-well plates at a density of 5x10^3/well. After 24 h, 48 h and 72 h, 20 µL of CellTiter 96® AQueous One Solution Cell Proliferation Assay (PROMEGA) were pipetted into each well. Plates were incubated at 37°C for 3-4 h in a humidified 5% CO_2 atmosphere. Absorbance was read at 490 nm using a multi-well plate reader (BioRadiMark^{TM}Microplate Reader). The obtained absorbance values were directly proportional to the number of viable cells in culture.

MTS assays were also applied for quantitative cell binding measurement after cell adhesion on coated substrates. HeLa and NIH-3T3 cells were diluted in serum-free medium, and seeded into uncoated and coated wells of TCT-PS, TCUT-PS and TCT-G 96-well plates described before, at a density of $5x10^4$/well. After incubation at 37 °C for 2 h, the unattached cells were aspirated gently with PBS, 200 µl of fresh serum-containing medium were added and MTS assay was immediately performed as described in the cell proliferation assay. Each MTS assay was performed at least in triplicate.

In cell spreading assays, HeLa and NIH-3T3 cells were diluted in serum-free medium, seeded at a density of 1.1×10^5/ well into uncoated, and Poly-L-Lysine (PLL) or HT-Pvfp-5β coated wells of an 8-well Nunc Lab-Tek II chamber slide. After incubation at 37°C for 2 h, the unattached cells were aspirated gently with PBS. The adhesion and spreading of cells were analyzed by actin filaments staining by using the green-fluorescent Alexa Fluor™ 488 Phalloidin (Invitrogen). Briefly, the adherent cells were fixed with 4% paraformaldehyde for 20 min, permeabilized with 0.5% Triton X-100 in PBS for 10 min and blocked for 30 min with 5% NGS (Sigma-Aldrich), 0.1% Triton X-100 in PBS. Alexa Fluor™ 488 Phalloidin (1:250) in blocking solution was added and incubated for 1 h in the dark. Then, cells were rinsed twice with PBS and stained with Hoechst 33342 fluorescent DNA-binding dye at 0.01 mg/mL at room temperature for 10 min. After rinsing three times with PBS, the chamber was removed and the slide sealed for the microscopic inspection. The nuclear morphology and cytoskeleton were observed on a Nikon Eclipse 80i microscope equipped for epifluorescence and recorded by a digital camera system.

Statistical analysis

Values obtained for the cellular analysis were reported as the mean of three independent experiments ± standard deviation (SD). Results were analyzed performing one-way analysis of variance, ANOVA, with pairwise comparisons made using Tukey's HSD test. Analyses were carried out using Sigmaplot 11.0 software (Systat Software Inc., San Jose, California, USA). Results were considered statistically significant at $P < 0.05$.

Structure modelling

To obtain a working structural model of Pvfp-5β we run a Blast search (https://blast.ncbi.nlm.nih.gov/Blast.cgi) in the PDB database with the Pvfp-5β sequence. The search identified the region between amino acid 288 and 368 of the 4xbm PDB entry as the closest hit having 47% sequence identify and an E-value of $1e^{-13}$. This is the X-ray crystal structure of the Notch ligand delta-like 1 protein. We then submitted the alignment to the SWISSMODEL server (https://swissmodel.expasy.org/) using our alignment.

Acknowledgements

We acknowledge support by a Dementia Research grant (RE1 3556), Patto per il Sud della Regione Siciliana - CheMISt grant (CUP G77B17000110001) and the Advanced Technologies Network Center of University of Palermo. This work was supported by the Francis Crick Institute through provision of access to the MRC Biomedical NMR Centre. The Francis Crick Institute receives its core funding from Cancer Research UK (FC001029), the UK Medical Research Council (FC001029), and the Wellcome Trust (FC001029).

Conflict of Interest Statement

The authors declare no conflict of interest.

References

1. Stewart RJ, Ransom TC, Hlady V. Natural Underwater Adhesives. J Polym Sci B Polym Phys. 2011;49(11):757-71.
2. Zhu W, Chuah YJ, Wang DA. Bioadhesives for internal medical applications: A review. Acta Biomater. 2018;74:1-16.
3. Jeon EY, Hwang BH, Yang YJ, Kim BJ, Choi BH, Jung GY, Chai HJ. Rapidly light-activated surgical protein glue inspired by mussel adhesion and insect structural crosslinking. Biomaterials. 2015;67:11-9.
4. Rahimnejad M, Zhong W. Mussel-inspired hydrogel tissue adhesives for wound closure. RSC Adv. 2017;7(75):47380-96.
5. Zhang X, Huang Q, Deng F, Huang H, Wan Q, Liu M, Wei Y. Mussel-inspired fabrication of functional materials and their environmental applications: Progress and prospects. Applied Materials Today. 2017;7:222-38.
6. Cha HJ, Hwang DS, Lim S. Development of bioadhesives from marine mussels. Biotechnol J. 2008;3(5):631-8.
7. Wilker JJ. Marine bioinorganic materials: mussels pumping iron. Current opinion in chemical biology. 2010;14(2):276-83.
8. Kord Forooshani P, Lee BP. Recent approaches in designing bioadhesive materials inspired by mussel adhesive protein. J Polym Sci A Polym Chem. 2017;55(1):9-33.
9. Lee H, Scherer NF, Messersmith PB. Single-molecule mechanics of mussel adhesion. Proc Natl Acad Sci U S A. 2006;103(35):12999-3003.
10. He Y, Sun C, Jiang F, Yang B, Li J, Zhong C, Zheng L, Ding H. Lipids as integral components in mussel adhesion. Soft Matter. 2018;14(35):7145-54.
11. Martinez Rodriguez NR, Das S, Kaufman Y, Israelachvili JN, Waite JH. Interfacial pH during mussel adhesive plaque formation. Biofouling. 2015;31(2):221-7.
12. Silverman HG, Roberto FF. Understanding marine mussel adhesion. Mar Biotechnol (NY). 2007;9(6):661-81.
13. Deming TJ. Mussel byssus and biomolecular materials. Current opinion in chemical biology. 1999;3(1):100-5.
14. Priemel T, Degtyar E, Dean MN, Harrington MJ. Rapid self-assembly of complex biomolecular architectures during mussel byssus biofabrication. Nat Commun. 2017;8:14539.
15. Yu J, Wei W, Menyo MS, Masic A, Waite JH, Israelachvili JN. Adhesion of mussel foot protein-3 to TiO2 surfaces: the effect of pH. Biomacromolecules. 2013;14(4):1072-7.
16. Rzepecki LM, Hansen KM, Waite JH. Characterization of a Cystine-Rich Polyphenolic Protein Family from the Blue Mussel Mytilus edulis L. The Biological bulletin. 1992;183(1):123-37.
17. Waite JH. Mussel adhesion - essential footwork. J Exp Biol. 2017;220(Pt 4):517-30.
18. George MN, Carrington E. Environmental post-processing increases the adhesion strength of mussel byssus adhesive. Biofouling. 2018;34(4):388-97.
19. Dove J, Sheridan P. Adhesive protein from mussels: possibilities for dentistry, medicine, and industry. Journal of the American Dental Association (1939). 1986;112(6):879.
20. Grande DA, Pitman MI. The use of adhesives in chondrocyte transplantation surgery. Preliminary studies. Bulletin of the Hospital for Joint Diseases Orthopaedic Institute. 1988;48(2):140-8.
21. Waite JH. Adhesion a la moule. Integrative and comparative biology. 2002;42(6):1172-80.
22. Cristian Sáez, Joel Pardo, Eduardo Gutierrez, Mónica Brito LOB. Immunological studies of the polyphenolic proteins of mussels. *Comp Biochem Physiol*. 1991;98B:569-572.

23. Zhang W, Yang H, Liu F, Chen T, Hu G, Guo D, Hou Q, Wu X, Su Y, Wang J. Molecular interactions between DOPA and surfaces with different functional groups: a chemical force microscopy study. RSC Advances. 2017;7(52):32518-27.
24. Maier GP, Rapp MV, Waite JH, Israelachvili JN, Butler A. BIOLOGICAL ADHESIVES. Adaptive synergy between catechol and lysine promotes wet adhesion by surface salt displacement. Science. 2015;349(6248):628-32.
25. Mirshafian R, Wei W, Israelachvili JN, Waite JH. alpha,beta-Dehydro-Dopa: A Hidden Participant in Mussel Adhesion. Biochemistry. 2016;55(5):743-50.
26. Yu M, Deming TJ. Synthetic Polypeptide Mimics of Marine Adhesives. Macromolecules. 1998;31(15):4739-45.
27. Yu M, Hwang J, Deming TJ. Role of l-3,4-Dihydroxyphenylalanine in Mussel Adhesive Proteins. *J Am Chem Soc*. 1999;121(24):5825-5826. doi:10.1021/ja990469y.
28. Ohkawa K, Nishida A, Yamamoto H, Waite JH. A glycosylated byssal precursor protein from the green mussel Perna viridis with modified dopa side-chains. Biofouling. 2004;20(2):101-15.
29. Hwang DS, Zeng H, Lu Q, Israelachvili J, Waite JH. Adhesion mechanism in a DOPA-deficient foot protein from green mussels(). Soft Matter. 2012;8(20):5640-8.
30. Jiang Z, Yu Y, Du L, Ding X, Xu H, Sun Y, Zhang Q. Peptide derived from Pvfp-1 as bioadhesive on bio-inert surface. Colloids Surf B Biointerfaces. 2012;90:227-35.
31. Guerette PA, Hoon S, Seow Y, Raida M, Masic A, Wong FT, Ho VH, Kong KW, Demirel MC, Pena-Francesch A, Amini S, Tay GZ, Ding D, Miserez A. Accelerating the design of biomimetic materials by integrating RNA-seq with proteomics and materials science. Nat Biotechnol. 2013;31(10):908-15.
32. Petrone L, Kumar A, Sutanto CN, Patil NJ, Kannan S, Palaniappan A, Amini S, Zappone B, Verma C, Miserez A. Mussel adhesion is dictated by time-regulated secretion and molecular conformation of mussel adhesive proteins. Nat Commun. 2015;6:8737.
33. Weisshuhn PC, Sheppard D, Taylor P, Whiteman P, Lea SM, Handford PA, Redfield C. Non-Linear and Flexible Regions of the Human Notch1 Extracellular Domain Revealed by High-Resolution Structural Studies. Structure. 2016;24(4):555-66.
34. Hwang DS, Zeng H, Masic A, Harrington MJ, Israelachvili JN, Waite JH. Protein- and metal-dependent interactions of a prominent protein in mussel adhesive plaques. J Biol Chem. 2010;285(33):25850-8.
35. Inoue K, Takeuchi Y, Miki D, Odo S. Mussel adhesive plaque protein gene is a novel member of epidermal growth factor-like gene family. J Biol Chem. 1995;270(12):6698-701.
36. Delaglio F, Grzesiek S, Vuister GW, Zhu G, Pfeifer J, Bax A. NMRPipe: a multidimensional spectral processing system based on UNIX pipes. Journal of biomolecular NMR. 1995;6(3):277-93.
37. Koppel DE. Analysis of Macromolecular Polydispersity in Intensity Correlation Spectroscopy: The Method of Cumulants. The Journal of Chemical Physics. 1972;57(11):4814-20.
38. Kershaw NJ, Church NL, Griffin MD, Luo CS, Adams TE, Burgess AW. Notch ligand delta-like1: X-ray crystal structure and binding affinity. Biochem J. 2015;468(1):159-66.
39. Kelly SM, Jess TJ, Price NC. How to study proteins by circular dichroism. Biochim Biophys Acta. 2005;1751(2):119-39.
40. Cooke RM, Wilkinson AJ, Baron M, Pastore A, Tappin MJ, Campbell ID, Gregory H, Sheard B. The solution structure of human epidermal growth factor. *Nature*. 1987;327(6120):339-341. doi:10.1038/327339a0
41. John A. Barltrop, Terence C. Owen, Ann H. Cory JGC. 5-(3-carboxymethoxyphenyl)- 2-(4,5-dimethylthiazolyl)-3-(4-sulfophenyl)tetrazolium, inner salt (MTS) and related

analogs of 3-(4,5-dimethylthiazolyl)-2,5-diphenyltetrazolium bromide (MTT) reducing to purple water-soluble formazans As cell-viability indicat. *Bioorg Med Chem Lett*. 1991;1(11):611-614.
42. Narhi LO, Arakawa T, McGinley MD, Rohde MF, Westcott KR. Circular dichroism of reduced and oxidized recombinant human epidermal growth factor. International journal of peptide and protein research. 1992;39(2):182-7.
43. Lim S, Choi YS, Song YH, Cha HJ. Salt Effects on Aggregation and Adsorption Characteristics of Recombinant Mussel Adhesive Protein fp-151. The Journal of Adhesion. 2009;85(11):812-24.

Table 1 – Mass spectrometry-based identification of cysteine-containing peptides generated by trypsin and chymotrypsin digestion of carboxyamidomethylated HT-Pvfp-5β.

Peptide	Experimental molecular weight	Theoretical molecular weight	Involved cysteines
24-31	996,409	996,405	Cys28-CAM*
(32-43)-(49-50)	656,281	656,255	Cys33-Cys49
35-40	635,282	635,270	Cys39-CAM*
(51-52)-(59-62)	801,333	801,305	Cys51-Cys60
(63-66)-(72-78)	1121,469	1121,404	Cy65-Cys76
(67-71)-(87-88)	568,326	568,303	Cys70-Cys87
(89-91)-(97-100)	869,374	869,356	Cys89-Cys98

* Carboxyamidomethylated cysteine

Figure legends

Figure 1. Structural prediction of the fold of HT-Pvfp-5β based on sequence similarity. A) Sequence alignment between Pvfp-5β (top) and the Notch ligand delta-like 1 protein (bottom). The sulfur bridges observed in Pvfp-5β are reported as lines on the top of the alignment, while the bridges observed in Notch ligand delta-like 1 are reported on the bottom. All the twelve

cysteines are conserved. B) The crystal structure of Notch ligand delta-like 1 protein (4xbm). The sulfur bridges observed in the Notch structure are indicated. C) Comparative model of Pvfp-5β using 4xbm as a structural template. The sulfur bridges observed experimentally by mass spectrometry are indicated either explicitly or with a discontinuous line for the pair Cys65-Cys76 that in the model is too far to be bridged.

Figure 2. Structural characterization of HT-Pvfp-5β. (A) CD spectrum of the protein in 5% acetic acid (pH 2.0), 0.1 M sodium acetate buffer (pH 4.0) and 0.1 M sodium acetate buffer (pH 5.6). The final concentration of the tested protein was 34 μM. All spectra were corrected by solvent subtraction. Spectra were collected after each new preparation of the protein (at least 12) to check reproducibility. B) portion of the homo-nuclear 2D NOESY spectrum. C) ^{15}N HSQC NMR spectrum of HT-Pvfp-5β. Both NMR spectra were recorded in H_2O/D_2O (95%/5% in volume) at pH 2.4, at 25 °C and 600 MHz.

Figure 3. Coating analysis of HT-Pvfp-5β on Polystirene and Glass surfaces. Cell-Tak and uncoated wells were used as positive and negative controls, respectively. The figure shows the Coomassie blue staining (left) and the relative densitometry analysis (right) of the coated proteins. The image is representative of five independent experiments.

Figure 4. Time course of light scattered intensity (I) and hydrodynamic radius (R) for a sample of HT-Pvfp-5β (protein concentration 5 μM) after changing the pH from 2.0 to 6.8 by addition of an appropriate amount of 0.1 M sodium bicarbonate at pH 8.3. The experiment was repeated on two independent sample preparations.

Figure 5. Cell viability of NIH-3T3 and HeLa cells grown on HT-Pvfp-5β coating using MTS assay. Three coating concentrations were used for HT-Pvfp-5β (1.75 μg/cm^2 Pvfp-5β 1; 3.5 μg/cm^2 Pvfp-5β 2; 7 μg/cm^2 Pvfp-5β 3). Uncoated surface was used as negative control. NIH-3T3 and HeLa cells in serum-containing medium were seeded at a density of 5x10^3/well and incubated for 72 h. Each value represents the mean of three independent experiments ±the standard deviation.

Figure 6. Cell adhesion of NIH-3T3 and HeLa cells on different surface materials coated with PLL or HT-Pvfp-5β. (A) tissue-culture treated glass plate TCT-G, (B) tissue-culture untreated

polystyrene plate TCUT-PS, (C) tissue-culture treated polystyrene plate TCT-PS. Two coating concentrations were used for HT-Pvfp-5β and Cell-Tak (3.5 μg/cm^2 Pvfp-5β 1 and Cell-Tak 1; 7 μg/cm^2 Pvfp-5β 2 and Cell-Tak 2), PLL was used as positive control at 7 μg/cm^2. NIH-3T3 and HeLa cells in serum-free medium were seeded at a density of 5x10^4/well and incubated for 2 h. Fold increase of cell amount is referred to the uncoated control for each surface material (dotted gray line). The effects were determined by the MTS assay. Each value represents the mean of three independent experiments ±SD. Statistical significance: *P < 0.05 vs. uncoated control.

Figure 7. Cell spreading of NIH-3T3 and HeLa cells on uncoated (UN), Poly-L-Lysine (PLL) or HT-Pvfp5β coated glass well. Fluorescent microscopy images of NIH-3T3 cells (A) and HeLa cells (B). Cell nuclei was in blue (Hoechst staining-DAPI channel) and F-actin was in green (Alexa Fluor™ 488 labelled phalloidin staining-FITC channel). Scale bar: 20 μm. Three independent experiments were performed.

Figure 1

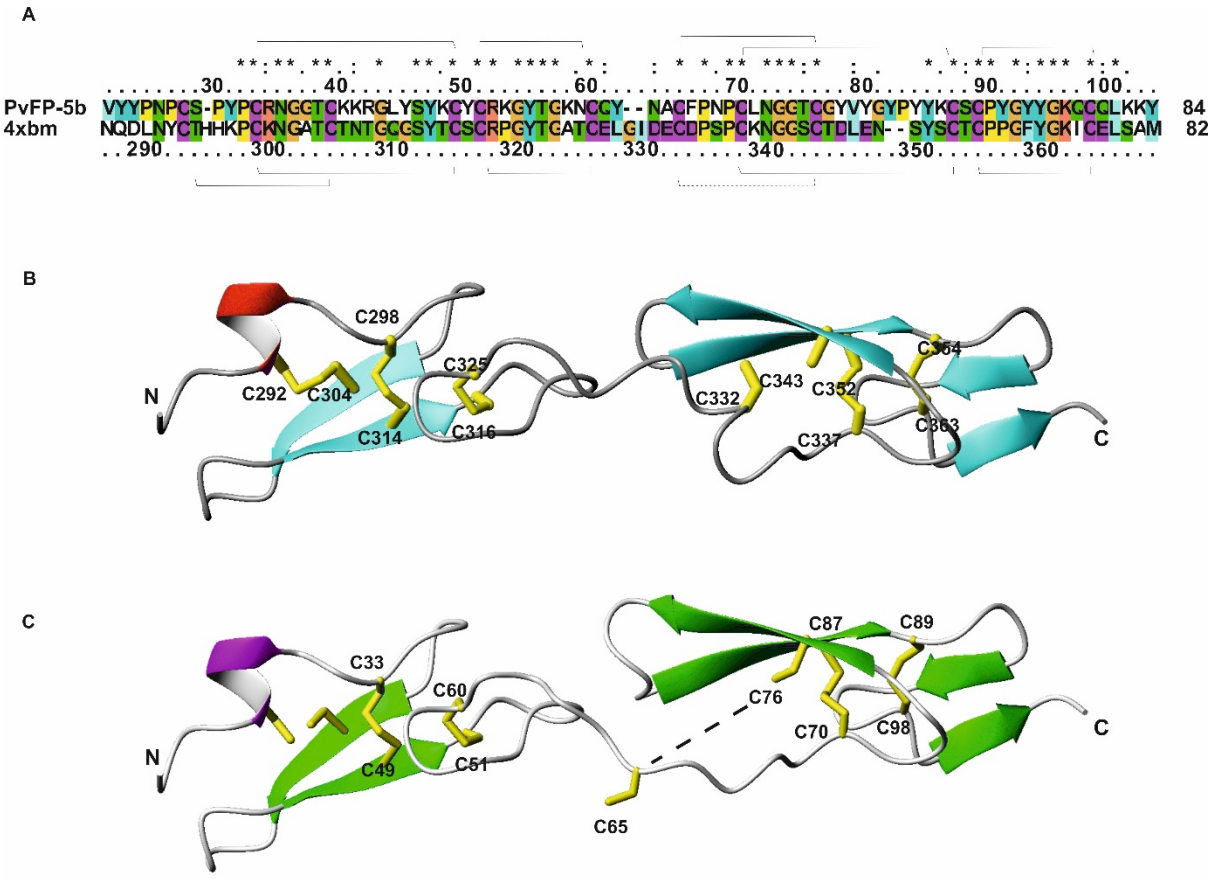

Figure 2

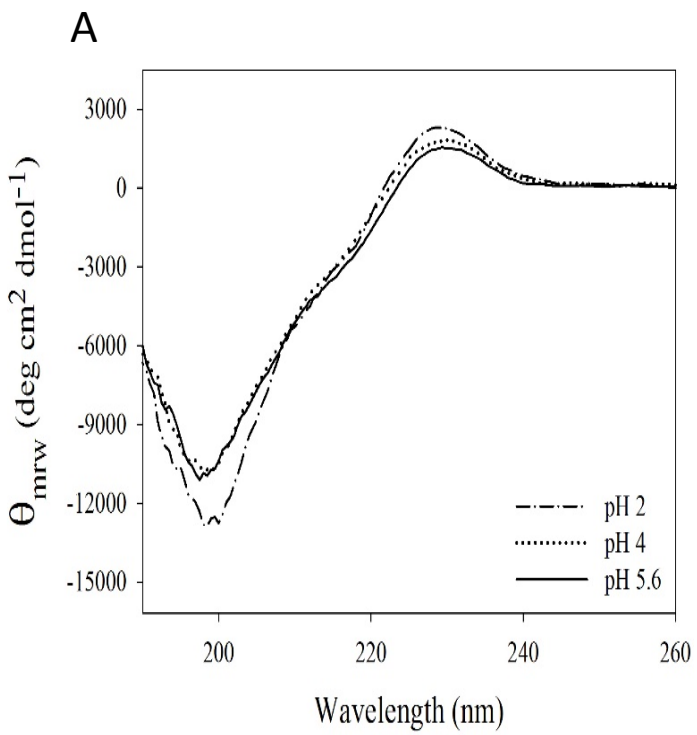

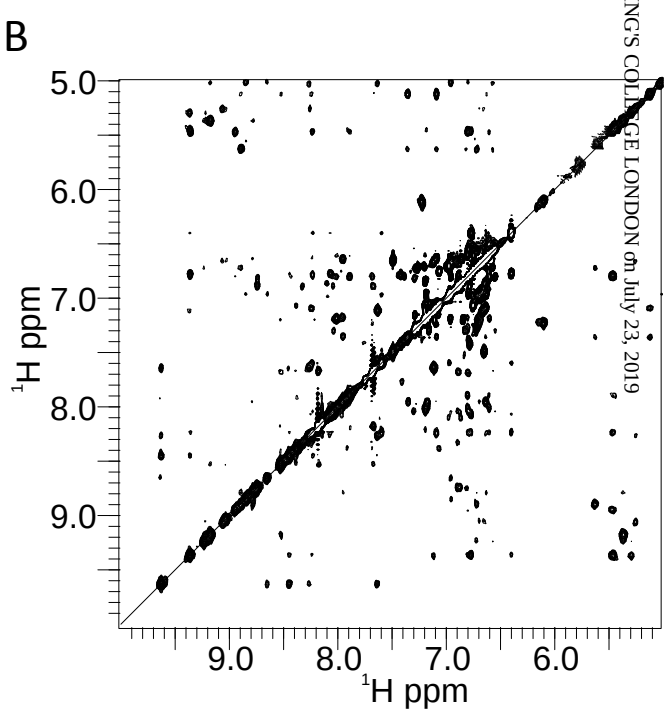

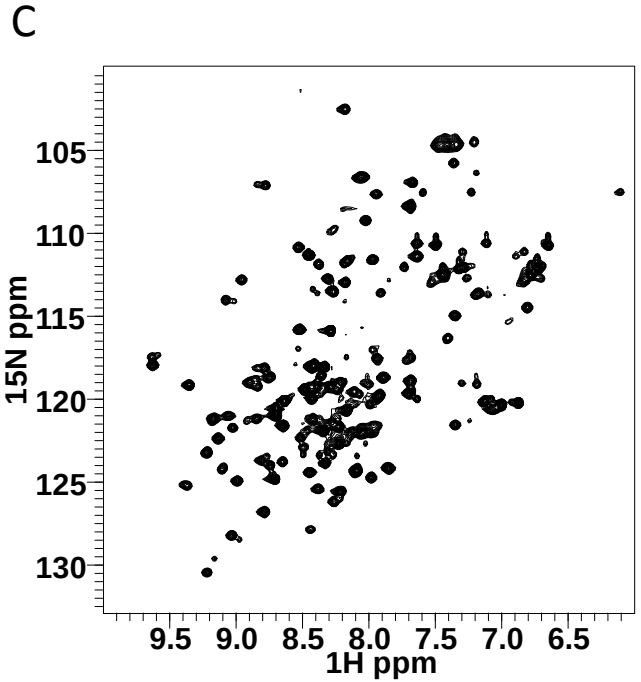

Figure 3

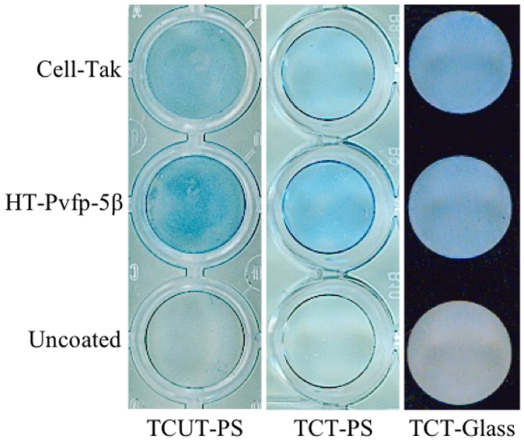

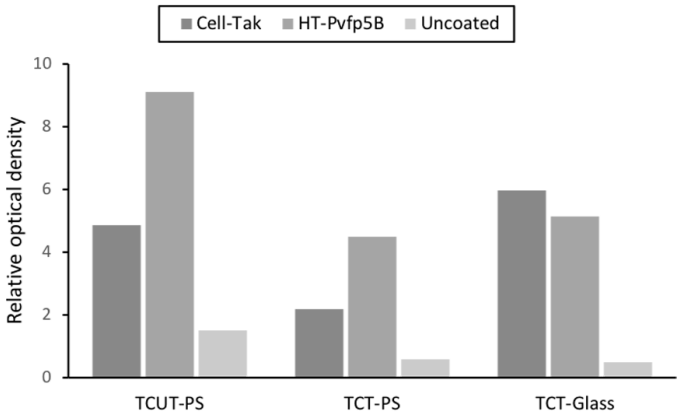

Figure 4

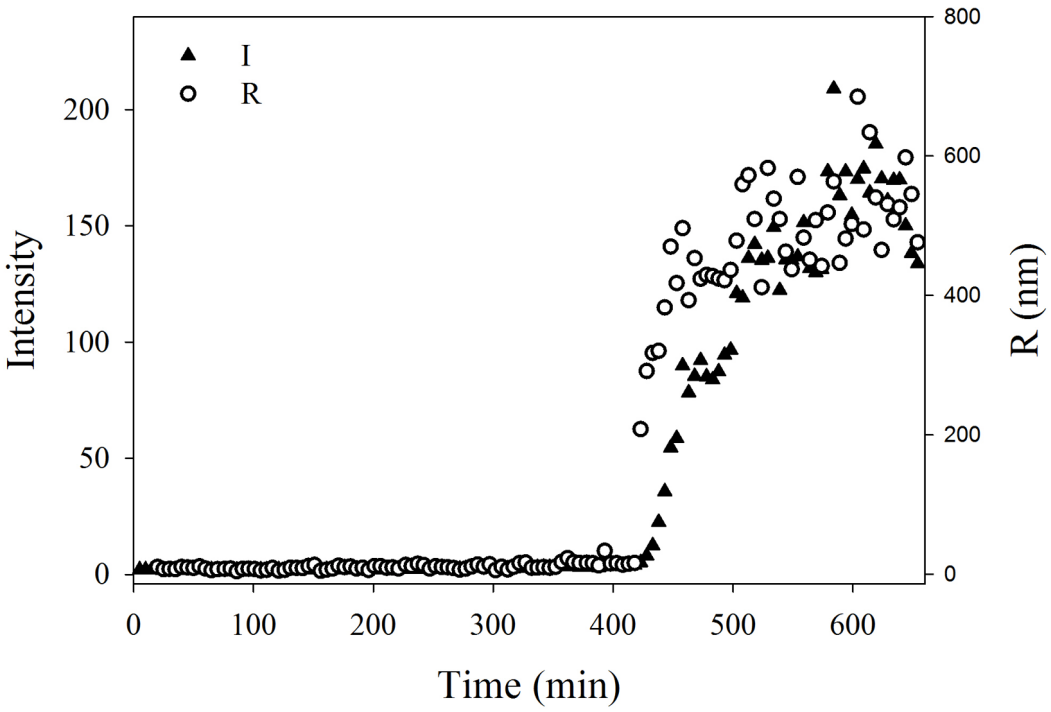

Figure 5

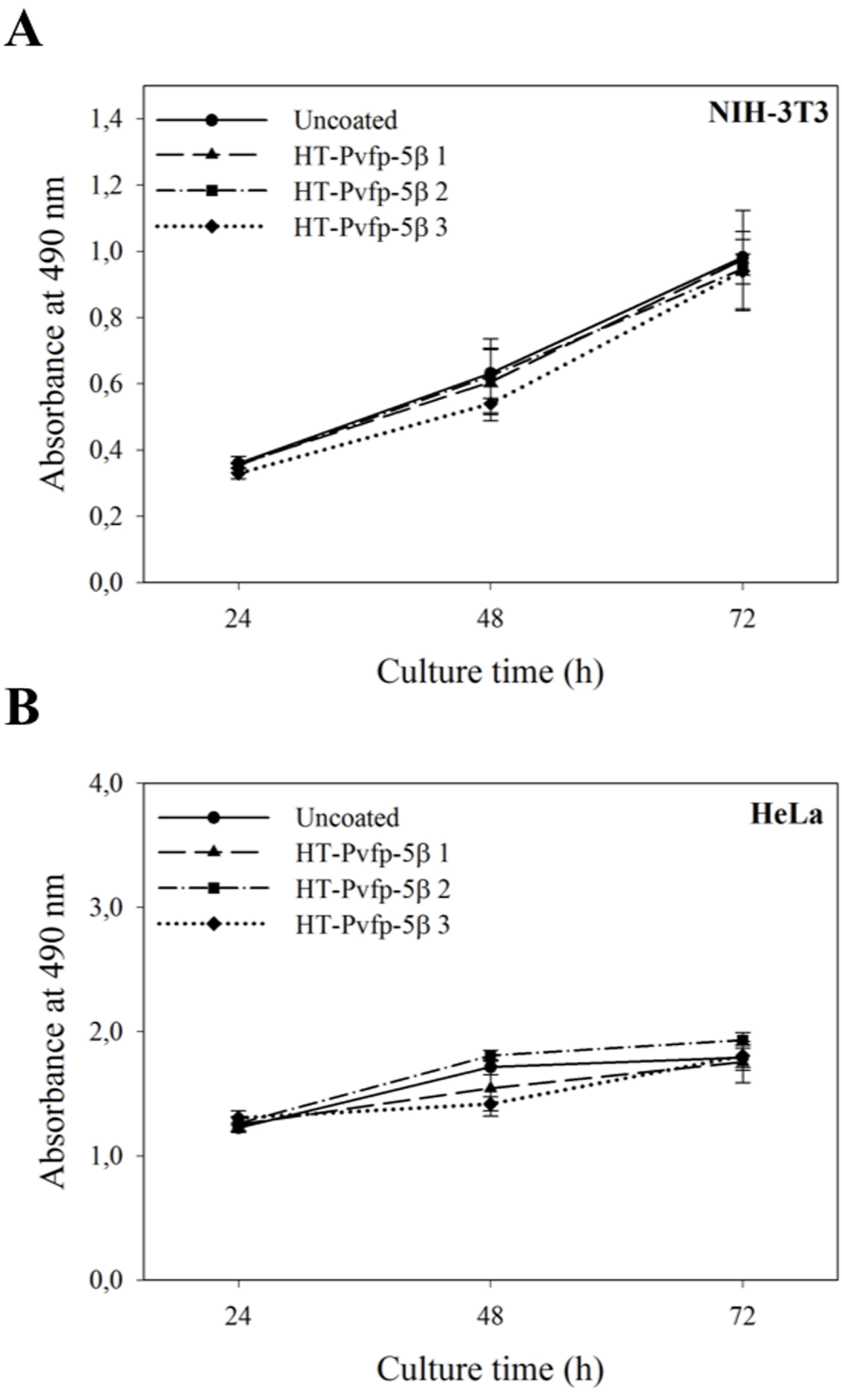

Figure 6

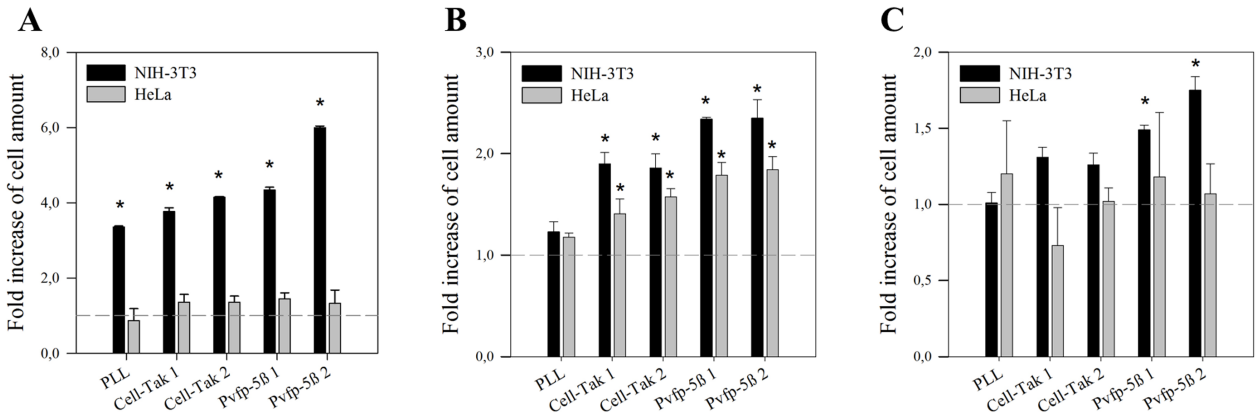

Figure 7

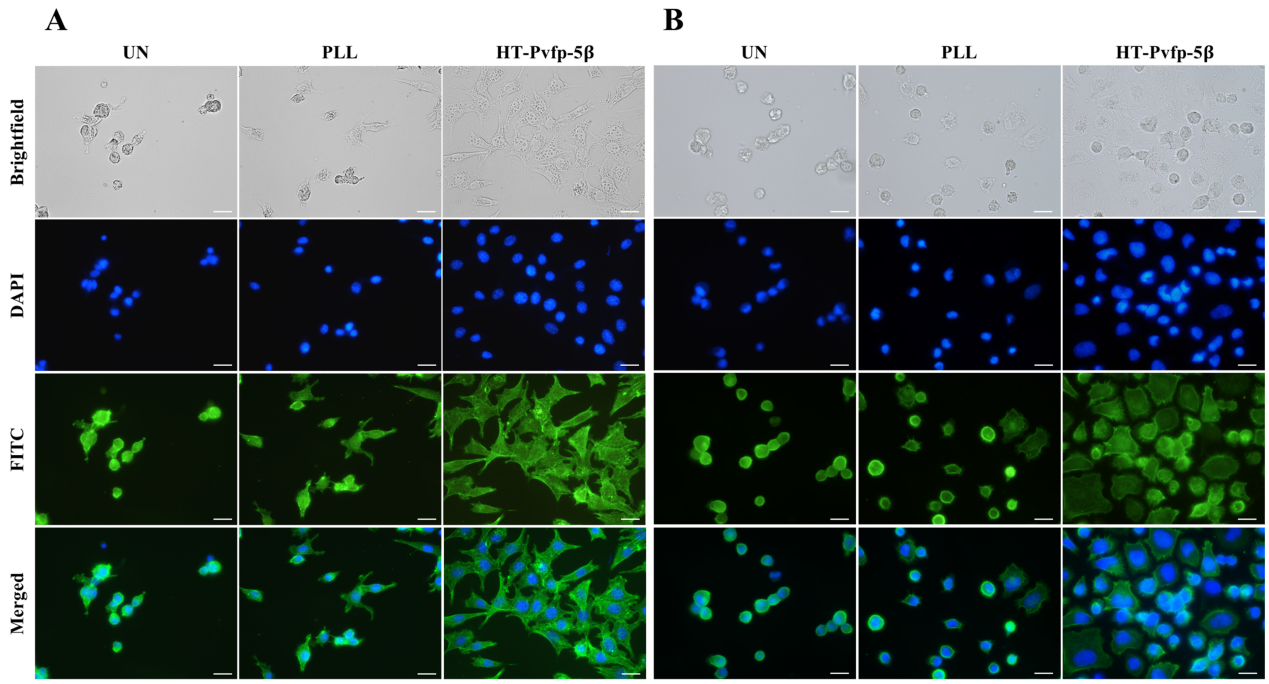

Recombinant mussel protein Pvfp-5β: a potential tissue bioadhesive

Radha Santonocito, Francesca Venturella, Fabrizio Dal Piaz, Maria Agnese Morando, Alessia Provenzano, Estella Rao, Maria Assunta Costa, Donatella Bulone, Pier Luigi San Biagio, Daniela Giacomazza, Alessandro Sicorello, Caterina Alfano, Rosa Passantino and Annalisa Pastore

J. Biol. Chem. published online July 10, 2019
